Microreactor for Acetone Deep Oxidation over Platinum

Fahima Rachedi, Richard Guilet, Patrick Cognet, Josiane Tasselli, Antoine Marty, Pascal Dubreuil

Fahima Rachedi[1]
Richard Guilet[1]
Patrick Cognet[1]
Josiane Tasselli[2]
Antoine Marty[2]
Pascal Dubreuil[2]

[1] Laboratoire de Génie Chimique, Université de Toulouse, Toulouse, France.

[2] Laboratoire d'Architecture et d'Analyse des Systèmes, CNRS, Université de Toulouse, Toulouse, France.

Microreactor for Acetone Deep Oxidation over Platinum

A catalytic, silicon-based, microstructured reactor was developed for the catalytic oxidation of volatile organic compounds, with the aim of small-scale localized air treatment. The microreactor was based on the stacking of microstructured platelets, and the active catalyst phase, i.e., platinum, was deposited onto the walls of the microchannels by the thermal evaporation technique. The experimental setup allowed testing the efficiency of the catalytic microreactor. The deep oxidation of acetone (as a target compound) in air was carried out at increasing temperatures, resulting in ignition curves. Wide ranges of inlet acetone concentrations (500–8000 ppmv) and space velocities (18,700–201,000 h^{-1}) were studied. Regarding acetone oxidation, the catalytic microreactor was found to exhibit high performances in terms of conversion, selectivity, and temperatures required to reach 50 and 95 % conversions.

Keywords: Catalytic oxidation, Microreactors, Waste air

1 Introduction

In recent years, microsystems such as heat exchangers or mixers have become of great interest for non-reactive processes. However, these microsystems have not yet offered all their industrial potentiality as microstructured reactors [1–3].

Typically, microreactors are microstructured devices featuring small channels in the range of micrometers. They can be constructed from microstructured plates enabling the fluid flow distribution over microchannels. Each microstructured platelet is typically made up of parallel microchannels with a width of the order of 50–500 µm and a width-to-depth ratio ranging from 1 to 100. As Kiwi-Minsker and Renken [4] underline in their review, microreactors offer very large surface-to-volume ratios ranging from 10,000 to 50,000 m^2/m^3, while the specific surface in conventional laboratory and production vessels is usually 100 m^2/m^3 and rarely exceeds 1000 m^2/m^3. The small dimension of the channels and the high surface-to-volume ratio ensure many properties of these devices and offer new possibilities for reaction pathways by achieving previously inaccessible residence times. They allow high heat and mass transfer and efficient fluid mixing [5, 6] as well as high adaptabilities in terms of process design by numbering up of microstructured elements.

Correspondence: Dr. R. Guilet (richard.guilet@iut-tlse3.fr), Laboratoire de Génie Chimique, Université de Toulouse, 4, allée Emile Monso, BP 74233, 31432 Toulouse cedex 4, France.

Regarding reaction processes, they enable a reduction of the time required to achieve complete conversion. Short residence times also reduce unexpected reactions of products and enhance the yield and selectivity. High heat transfer properties enable high control of temperature, facilitating isothermal processes, preventing hot-spot formation and avoiding thermal runaway, especially when the occurring reactions involve high exothermicity. Thus, microreactors can offer some advances in catalytic processes. Furthermore, due to the characteristic dimensions of the microchannels, microstructured devices enable a large decrease in the distance between the catalytic zone and the stream, with more efficient heat and mass exchange properties than for conventional packed-bed reactors. Catalytic microstructures and subsequent flow control allow a more secure manipulation of hazardous, inflammable and even explosive products, which is not possible in conventional reactors. Recently, the applications of microreactors to catalytic reactions were reviewed by Kiwi-Minsker and Renken [4]. Although the use of microreactors for catalytic reactions offers clear advantages, the authors conclude that the introduction of the solid catalyst remains a difficulty and that catalytic wall microreactors are more suitable. Moreover, Kolb and Hessel [7] give an overview of the work and research interests in the field of catalytic gas phase reactions. Many examples using various technologies are reported, such as oxidations, hydrogenations, dehydrogenations, dehydrations, and reforming processes. Among them, deep or partial catalytic oxidation is of great interest for many applications, including oxidation for air treatment.

Removal of air pollutants such as volatile organic compounds (VOC) is a major health and environmental concern. European directives indeed tend to regularly decrease the authorized pollutant emission levels. VOC include a wide variety of chemicals: aliphatic and aromatic hydrocarbons, halogenated hydrocarbons, aldehydes, ketones, alcohols, glycols, ethers, epoxides, phenols, etc. The three major sources of VOC are: power generation (20 %), vehicle emissions (40 %), and solvents for industrial purpose (27 %) [8]. They are commonly found in the atmosphere at a high level in all urban and industrial centers. They actively take part in the increase of the greenhouse effect, and a carcinogenic effect is also assigned to some of them [9, 10]. The large variety of sources and compounds with different physical and chemical properties has led, over the years, to the development of a wide range of VOC treatment processes [11]: bioprocesses (biofilters), chemical processes (combustion, ozonation, photooxidation), and physical processes (condensation, adsorption, absorption). Actually, the main processes are adsorption- and/or combustion-based systems. The first is a non-destructive process and needs a subsequent treatment of the adsorbent, and the second process usually occurs at high temperatures (about 1200 °C) in order to avoid the formation and release of hazardous by-products, such as dioxins, but produces high levels of nitrogen oxides (NO_x), which eventually requires further treatment [12].

In the last several years, catalytic oxidation has become an alternative destructive process of VOC that offers many advantages, such as high combustion efficiency and extremely low emissions of NO_x and unburnt hydrocarbons. Compared to thermal combustion, the reaction occurs at lower temperatures, between 200 and 500 °C, which is of very great interest from energy, security and operation cost points of view. Regarding the catalyst performances, various catalytic materials, such as noble metals (Pt, Pd) and mixed oxides (V, Mn, Co, Cu, Cr), supported or not on oxides (e.g. alumina), have been shown to be efficient for VOC oxidation [13–15]. Platinum-based catalysts are considered as being among the most active catalysts for VOC deep oxidation [16–18].

Although heterogeneous catalytic deep oxidation of VOC is a quite well-known process [19], its application to air treatment is nowadays limited to large-scale units. The major difficulty is often linked to the multiple pollution sources and subsequently the necessity of collecting all of the polluted effluents towards a large-scale treatment unit. In fact, much of the industrial air pollution comes from enclosed sources. Processes that could easily adapt and fit to various localized pollution sources, whatever the pollutants, the flow and the application, would be a great technological advance in air pollution treatment. In the field of small-scale localized air treatment, the main limitation is the inherent difficulty in designing and sizing the reactor for these applications.

Thus, catalytic microsystems could be implemented for the removal of volatile organic compounds in various industrial environments such as drying, painting, varnishing and dry-cleaning workshops. As mentioned above, they offer the advantage of being adaptable by numbering up of small units, and they consequently allow the design of appropriate catalytic processes whatever the scale and the effluent. Moreover, while the catalytic oxidation processes are generally carried out in a catalytic fixed-bed reactor with an inflammation risk of the catalytic bed because of hot-spot formation, microreactors offer new advances as they allow heat to be transferred or removed very easily and efficiently [20].

In this work, the performances of a silicon-based microstructured reactor for catalytic oxidation of acetone are presented. Acetone was chosen as a representative volatile organic compound because it is both a widespread VOC and one of the most difficult to oxidize [8]. The catalytic activity of the microreactor was tested for a wide range of inlet concentrations and various space velocities.

2 Microstructured Reactor

The experiments were carried out in a microreactor designed according to the characteristics of the reaction and based on the stacking of microstructured platelets. The core part of the reactor was composed of 12 stacked platelets (30 × 30 mm) held by screws in a cylindrical inner housing. The whole was embedded in a stainless-steel outer housing equipped with four electrical resistive cartridges allowing heating of the reactor (see Figs. 1, 2).

One advantage of the proposed reactor is its modularity: The platelets were inserted in the inner housing recess and could be easily removed and replaced, allowing various configurations (microchannels geometry and/or platelets length) to be tested.

The platelets were fabricated from silicon wafers with 525 µm thickness: *(i)* Silicon is an interesting material in terms of heat transfer, with high conductibility allowing heat release from the reactor core; *(ii)* moreover, microtechnologies offer the possibility to structure the silicon material in surface and

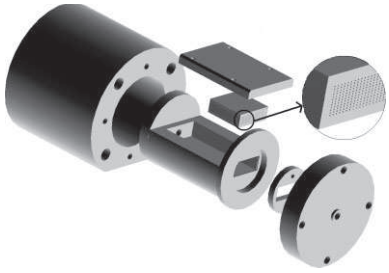

Figure 1. Explosion view of principal elements of the microreactor.

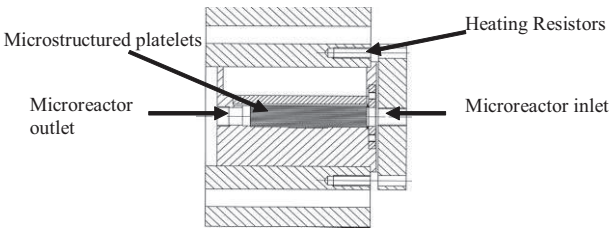

Figure 2. Microreactor scheme.

depth. It is possible to obtain channels of various depths and widths in a reproducible way. In the present paper, only one set of platelets was used (see Tab. 1).

Table 1. Characteristics of the microreactor.

$S_{channel}$ [mm^{2}]	42
$V_{channel}$ [mm^{3}]	3
n	12
N	300
S_{tot} [mm^{2}]	12,600
V_{tot} [mm^{3}]	900
S/V [m^{2}/m^{3}]	14,000

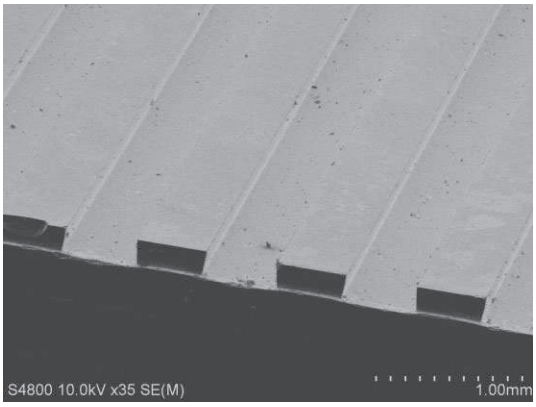

Figure 3. View (scanning electron microscopy) of microchannels obtained by DRIE after Pt deposition.

Each of the 12 platelets was made up of 29 parallel microchannels of 200 µm width, microstructured by the deep reactive ion etching (DRIE) technique according to the Bosch process, i.e. a cyclic repetition of an ion-assisted etching of the silicon substrate by an etching gas (SF_6) and a sidewall passivation using a polymer-producing gas (C_4F_8) [21]. After a thermal oxidation step in order to recover the silicon surface by a thin oxide layer (0.1 µm), the active catalyst phase was deposited on the walls of the microchannels (see Fig. 3). The selected material, platinum (Pt), which is well known for its catalytic potentialities in gas phase reactions, was deposited by the thermal evaporation technique, allowing large-scale fabrication and good reproducibility of the catalyst layer thickness (about 130 nm). The mean roughness of the microchannel surface was evaluated by atomic force microscopy. After catalyst deposition, the roughness was about 10 nm.

Regarding the gas feed, the gas stream was introduced from the inlet tube to the platelets stack via a diffuser (a drilled plate distributor associated with a diffusion chamber).

The evaporation cell was fed with a gaseous stream composed of synthetic air (80 % N_2, 20 % O_2) 5.6 from Linde Gas, controlled by mass flow meters (5850 TR Series Brooks®). The required acetone liquid flow was calculated according to the air flow to reach the desired concentration. Before being introduced into the microstructured reactor, the gaseous acetone-air mixture was formed in the evaporation cell at 200 °C; the evaporator was equipped with a heating resistor. A cylindrical grill and a capillary tube within the cell ensured the homogeneity of the gas flow at the inlet of the microreactor. A thermocouple at the outlet of the evaporator and a PID regulator allowed the temperature to be controlled. The microreactor was equipped with two thermocouples; one was placed in the stainless steel outer housing and the other one was placed just at the end of the platelets, which allowed the control of the reaction temperature.

The inlet and outlet of the microreactor were connected to an on-line gas phase chromatography (GPC) apparatus (CP3800) from Varian. The GPC system was equipped with

3 Experimental

The main goal of the experiments was to determine the efficiency of the microreactor for VOC deep oxidation. The present work dealt with studying acetone conversion versus temperature for various inlet acetone concentrations and air flows. The experimental setup is shown in Fig. 4.

With a 10-mL glass syringe (Hamilton Gastight®) with PTFE plungers, liquid acetone (Chromosolv®, ≥99.9 %; Sigma Aldrich) was injected into an evaporation cell through a capillary tube, by using a syringe pump (PH 2000 Infusion) from Harvard Apparatus, which allowed getting the required low liquid flows (a few milliliters of acetone per hour).

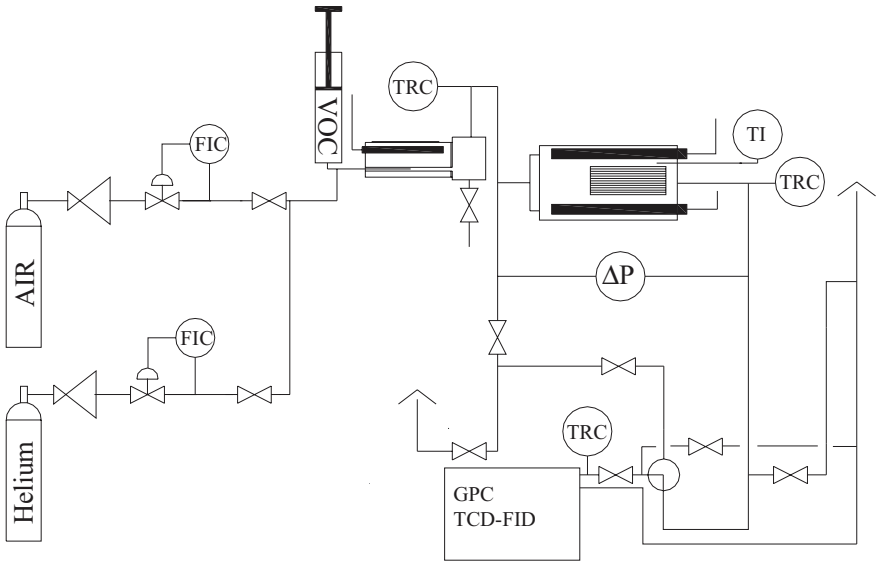

Figure 4. Scheme of the experimental setup.

both a thermal conductivity detector (TCD) and a flame ionization detector (FID), to enable the analysis of all gaseous components. Thus, the on-line analytical equipment allowed simultaneous monitoring of the VOC concentration at the inlet and outlet, and of the potential products of the reaction, such as H_2, CO, CH_4, CO_2, C_2H_4 as well as N_2 and O_2. Before testing the activity of the catalytic microstructured platelets, the catalyst was activated in situ at 450 °C for 8 h under a constant air flow. After the first run, the temperature of the catalyst was maintained at 550 °C, the highest reaction temperature, for a few hours. The experimental assessment of catalytic activity was carried out by scanning the operating temperature and the gas flow as well as the VOC concentration. The ranges of the parameters are given in Tab. 2. Mass flow controllers were used to prepare the feed mixture. The VOC concentration range was established according to the authorized levels of pollutant emissions and the inlet air flow. The corresponding liquid feed rate was controlled by the syringe pump, and the VOC liquid flow was calculated assuming that the evaporation cell was efficient enough to vaporize all the liquid.

Table 2. Operating parameters.

Air flow range [NL/h]	16.8, 31.2, 61.2, 181.2
Concentration range [ppmv]	500, 2000, 4000, 8000
Temperature [°C]	200–550

Before each run, the VOC inlet concentration was determined on-line by GC after the steady state was reached at the evaporator outlet. The inlet concentration deviation was considered acceptable when not exceeding 5 %. For a given concentration and a fixed gas flow, the operating temperature was increased from 200 to 500 °C by steps of 25 °C. For each temperature, the outlet stream was analyzed after the steady state was established. The experiments were conducted at atmospheric pressure. The ignition curves were constructed by following both VOC disappearance and CO_2 appearance.

Regarding the flow behavior within the microreactor, the mean residence time is the total volume of the microchannels divided by the total inlet gas flow rate, corrected to the operating temperature and pressure of the gas stream in the reactor. The inlet air flow rate was here metered with a mass flow controller set to standard conditions. For each experiment, the flow rate within the microreactor was corrected to the operating conditions assuming that the ideal gas law is valid. Thus, the mean residence time decreases by about 60 % when the temperature increases from 200 to 500 °C. With regard to the operating temperature used in this work, the mean residence times ranged from 7 to 120 ms. Moreover, the hourly space velocities were calculated to compare the experimental results. The hourly space velocity is indeed widely used in the catalysis literature and is commonly defined as the ratio of the gas feed volume flow rate (measured at standard temperature and pressure) over the catalyst volume or weight. In this paper, the gas hourly space velocity (GHSV; in h^{-1}) was defined as the ratio of the total air inlet flow rate at standard conditions over the total volume of the microchannels. It is actually the inverse of the mean residence time. The GHSV ranged from about 18,700 to 201,000 h^{-1}.

4 Results and Discussion

The efficiency of the catalytic microreactor for acetone oxidation was studied by obtaining the light-off curves (conversion versus temperature). Experimental points were obtained by increasing the temperature. The reactivity of the system was both established according to the shape of the light-off curves and in terms of T_{50} and T_{95}, meaning the temperatures at which conversions reach 50 and 95 %, respectively. These parameters were obtained from the light-off curves.

4.1 Conversion Calculation

All experiments, whatever the operating parameters, allowed observing that CO_2 was the only reaction product detected. Actually, water was not measured. GPC allowed determining the acetone and carbon dioxide concentrations in the outlet stream, C_{out} and C_{CO_2}, respectively. The acetone conversion was calculated by following both the VOC disappearance and the CO_2 appearance, and by using the mass balance in relation with the reaction scheme:

$$H_3C\text{–}CO\text{–}CH_3 + 4O_2 \xrightarrow{Pt} 3CO_2 + 3H_2O$$

The mass balance on acetone for the reaction, in terms of molar flow, gives:

$$F_{in} = F_{out} + F_{CO_2}/3 \tag{2}$$

Since the microreactor could be considered as almost isothermal and since the VOC concentrations were very low in the gas stream, the total volume and molar flows were regarded as constant throughout the reactor. Thus, Eq. (1) was written in terms of concentrations as:

$$C_{in} = C_{out} + C_{CO_2}/3 \tag{3}$$

From the measured inlet and outlet concentrations, acetone conversions were calculated according to both outlet acetone concentration (acetone disappearance) and outlet carbon dioxide concentration (CO_2 appearance), i.e. $X_{/Acetone}$ and $X_{/CO_2}$, respectively:

$$X_{/Acetone} = 1 - \left(\frac{C_{out}}{C_{av}}\right) \tag{4}$$

$$X_{/CO_2} = \left(\frac{C_{CO_2}/3}{C_{av}}\right) \tag{5}$$

where C_{av} was actually the average of the measured inlet acetone concentration. $X_{/Acetone}$ and $X_{/CO_2}$ should be equal, according to the mass balance. However, as the inlet concentration could undergo variations according to the efficiency of

the evaporator, and since the mass balance was verified, the inlet concentration, C_{in}, was calculated using the mass balance (Eq. 3) for each oxidation temperature (experimental points). Thus, the acetone conversion was calculated from Eq. (6) avoiding the influence of the inlet concentration variation:

$$X = \frac{C_{in} - C_{out}}{C_{in}} \quad (6)$$

4.2 Ignition Curves

Figs. 5–8 show the conversion of acetone into CO_2 versus oxidation temperature at various inlet concentrations as a function of the space velocity ranging from 18,700 h^{-1} over 35,000 and 68,000 h^{-1} to 201,000 h^{-1}. The figures gather the results of the experiments with similar inlet concentrations. The concentrations given in the legend are the inlet target concentrations, whereas the ones indicated in brackets are the inlet acetone concentrations measured when steady state was established.

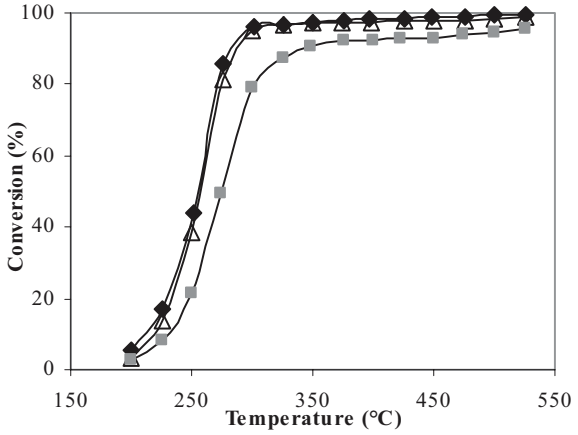

Figure 5. Ignition curves for 8000 ppmv. (■) 68,000 h^{-1} (8290 ppmv), (Δ) 35,000 h^{-1} (8547 ppmv), (◆) 18,700 h^{-1} (7787 ppmv).

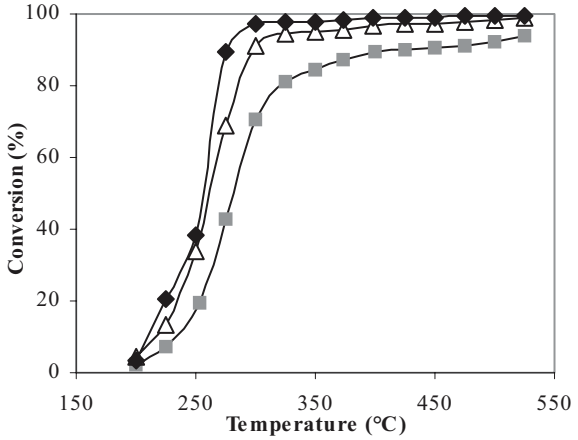

Figure 6. Ignition curves for 4000 ppmv. (■) 68,000 h^{-1} (3947 ppmv), (Δ) 35,000 h^{-1} (3947 ppmv), (◆) 18,700 h^{-1} (3865 ppmv).

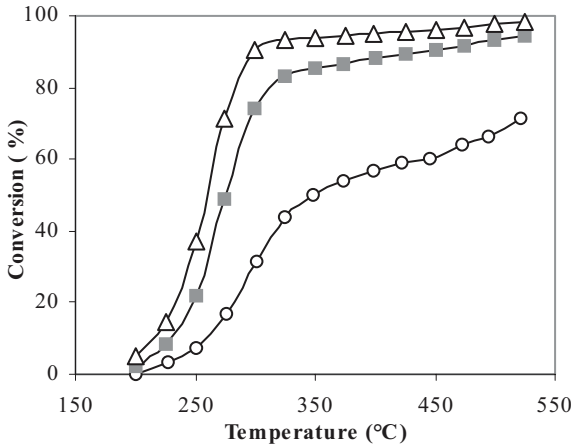

Figure 7. Ignition curves for 2000 ppmv. (○) 201,000 h^{-1} (2225 ppmv), (■) 68,000 h^{-1} (2198 ppmv), (Δ) 35,000 h^{-1} (2213 ppmv).

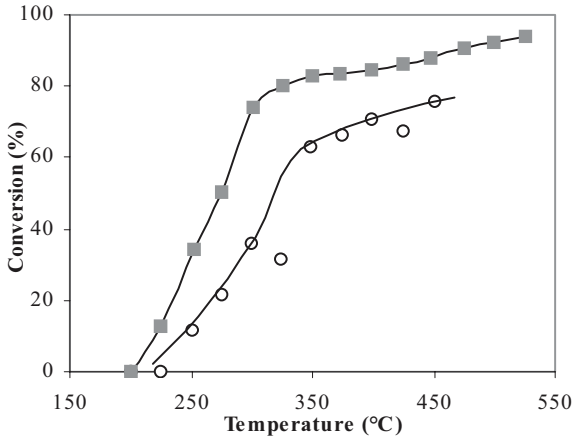

Figure 8. Ignition curves for 500 ppmv. (○) 201,000 h^{-1} (490 ppmv), (■) 68,000 h^{-1} (483 ppmv).

Regarding the highest concentration studied (see Fig. 5), acetone oxidation starts from 200 °C, and almost complete conversion (97 %) of acetone into CO_2 is obtained at 350 °C for the 18,700 h^{-1} space velocity. It must be repeated here that CO_2 and water were the only products formed under the experimental conditions used. No carbon monoxide was detected under any of the experimental conditions. Moreover, it is observed that higher space velocities lead to similar results, although the results tend to underline that the conversion decreases slightly when space velocity rises. The same behavior is observed in Figs. 6 and 7 for 4000 and 2000 ppmv inlet concentration. However, in Fig. 7, one observes that the conversion at 350 °C does not exceed 85 and 50 % when the space velocities are 68,000 and 201,000 h^{-1}, respectively. For the lowest concentration, i.e. 500 ppmv, Fig. 8 displays similar results. Although acetone conversion increases obviously with temperature, it does not exceed 94 % even at 525 °C when GHSV = 68,000 h^{-1}.

Nevertheless, one run (not represented here) at 35,000 h^{-1} for a nearby concentration, i.e. 615 ppmv, exhibits much higher conversions, more than 90 % at 325 °C and 98 % at 525 °C.

These results can also be compiled with other experiments in terms of temperatures required to reach 50 and 95 % conversions, i.e. T_{50} and T_{95}, respectively. It can be seen from Fig. 9 that the temperatures required for 50 % conversion do not much depend on the concentration, whatever the inlet concentration and for the two space velocities reported. Whatever the experimental conditions (i.e. concentration and space velocity), T_{50} is near 270 °C, although a slight increase is observed when the space velocity increases: T_{50} ranges from 260 °C at 18,700 h^{-1} to near 300 °C at 201,000 h^{-1} (see Fig. 10). Fig. 10 highlights the expected influence of the space velocity: Oxidation needs higher temperatures to be completed when the space velocity increases. Regarding the temperature required to reach 95 % conversion, Fig. 9 exhibits a different behavior according to space velocity. At 68,000 h^{-1}, T_{95} is not only higher, but also does not depend on the inlet concentration. This could be explained with an apparent first-order process. However, T_{95} obviously decreases at 35,000 h^{-1} with increasing concentration. This could arise from mass transfer limitations. Indeed, at 35,000 h^{-1}, the mean residence time is about twice higher than at 68,000 h^{-1} and a much lower T_{95} is reasonably expected whatever the inlet concentration. Thus, a diffusion limitation could explain the higher T_{95} observed for the lowest concentration. Further work is in progress to study the influence of the size (depth and width) of the microchannels on the conversion of acetone.

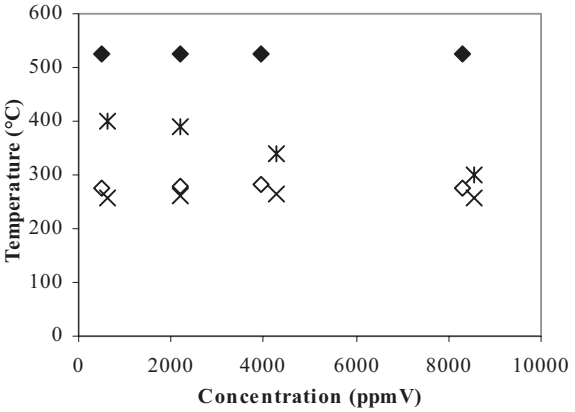

Figure 9. Temperatures required for 50 and 95 % conversion (T_{50} and T_{95}) versus inlet acetone concentration. 35,000 h^{-1}: (×) T_{50}, (✳) T_{95}; 68,000 h^{-1}: (◇) T_{50}, (◆) T_{95}.

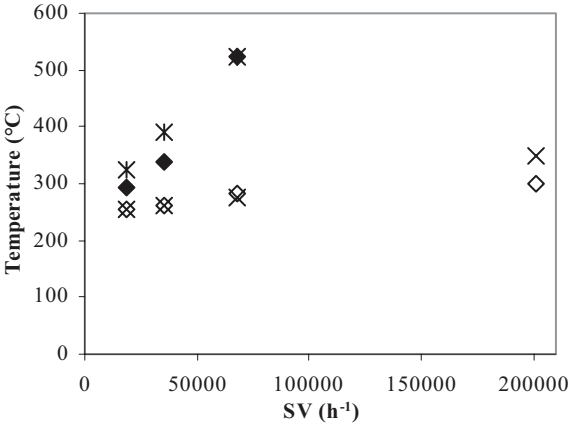

Figure 10. Temperatures required for 50 and 95 % conversion (T_{50} and T_{95}) versus space velocity. 4000 ppmv: (×) T_{50}, (✳) T_{95}; 2000 ppmv: (◇) T_{50}, (◆) T_{95}.

With regard to the literature on catalytic oxidation of acetone over platinum-based catalysts, our results are promising. Gil [17] found complete conversion of acetone at 352 °C using platinum on a clay-based support at a GHSV of about 34,000 h^{-1}. Regarding low concentrations, Burgos [22] performed oxidation of 225 ppmv acetone over a $Pt/Al_2O_3/Al$ monolith at a GHSV of 3680 h^{-1}. According to the reported ignition curves, T_{50} was about 210 °C and complete conversion was reached at 340 °C. These temperatures are obviously lower than those of Fig. 8, even at a lower inlet concentration. However, one must underline that the GHSV values of our study are more than ten times higher than the above-mentioned one. This fact is emphasized by the data obtained by Sharma [23]. The oxidation of acetone at 400 °C using a Pt-loaded hydrophobic catalyst did not yield more than 80 % conversion, with inlet concentrations ranging from 550 to 2350 ppmv and with GHSV values ranging from 3000 to 15,000 h^{-1}. Moreover, a comparison with the above-mentioned results must be considered with regard to the nature of the catalyst support. Although the catalyst is the same, Pt deposited by the thermal evaporation technique might exhibit a different activity than a Pt-catalyst supported on clay or alumina.

4.3 Effect of O_2 Concentration on Acetone Oxidation

In order to evaluate the effect of oxygen, experiments for a given stream flow and concentration were carried out at different oxygen concentrations in the inlet gas stream: 10 and 20 %. The 10 % concentration was obtained by mixing the air stream with a stream of helium (50 % in volume), maintaining the total gas flow rate. The experiments were conducted at 2000 ppmv and at a GHSV of 68,000 h^{-1}, and the light-off curves were achieved and are presented in Fig. 11. The acetone conversions are slightly higher when the oxygen concentration decreases. The difference is especially obvious between 225 and 300 °C, and T_{50} decreases from 275 to 265 °C when the oxygen concentration decreases from 20 to 10 %.

Even if the negative effect of oxygen does not clearly appear from these two experiments, it is in accordance with the literature. Indeed, this effect is commonly observed when VOC catalytic oxidation is performed using a supported Pt catalyst. The catalytic oxidation of methyl-isobutyl-ketone over a Pt/zeolite catalyst exhibits maximum conversion with 8 % oxygen in the feed [24]. This was also reported by Papaefthimiou [15] for the oxidation of butanol with a $Pt/\gamma\text{-}Al_2O_3$ catalyst, and a kinetic study allowed determining a negative reaction order with respect to oxygen. Although a high oxygen concentration tends to inhibit the reaction, from a process point of view it is preferable to operate the VOC oxidation with air.

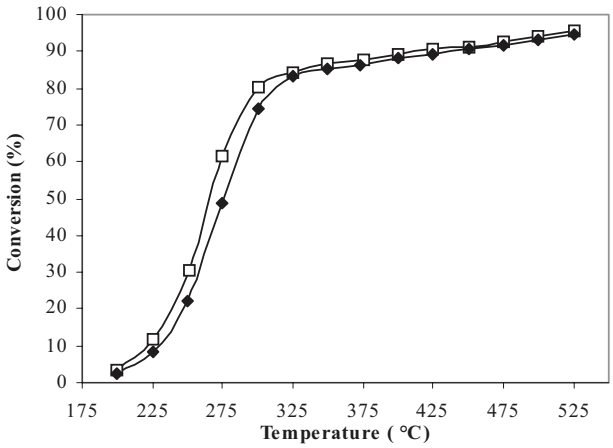

Figure 11. Influence of O_2 concentration on ignition curves at 68,000 h^{-1}. (□) 10 % O_2 (2198 ppmv), (◆) 20 % O_2 (2083 ppmv).

5 Conclusions

A catalytic silicon-based microstructured reactor was designed for the treatment of VOC-containing air streams. The design was based on the stacking of silicon microstructured platelets with platinum as the active catalyst phase. The performance of the microreactor for catalytic oxidation of acetone was tested. Ignition curves were determined from acetone disappearance and carbon dioxide formation with increasing temperatures. Outlet stream analysis coupled with mass balance showed that no by-products were obtained. According to inlet acetone concentrations ranging from 500 to 8000 ppmv, the catalytic activity reached more than 95 % conversion, depending on the operating space velocity. The decrease of the inlet concentration and/or the rise of the space velocity resulted in a loss of efficiency, possibly due to diffusion limitations. Moreover, the determination of T_{50} and T_{95}, the temperatures required to reach 50 and 95 % conversion, respectively, highlighted, under the operating conditions, that T_{50} did not much depend on the inlet concentration.

The results showed that the catalytic phase was very active for acetone deep oxidation. The effectiveness of the designed microreactor is promising. However, other relevant experiments should be carried out and added to prove the feasibility of the process and the real efficiency of the microsystem for catalytic oxidation of volatile organic compounds with the aim of small-scale localized air treatment. Investigations are in progress regarding the efficiency of the catalytic microreactor toward the degradation of other VOC.

The authors have declared no conflict of interest.

Symbols used

C_{av}	[ppmv]	average inlet concentration of acetone (steady state)
C_{CO2}	[ppmv]	outlet concentration of carbon dioxide
C_{in}	[ppmv]	inlet concentration of acetone
C_{out}	[ppmv]	outlet concentration of acetone
F_{CO2}	[mol/s]	outlet molar flow of carbon dioxide
F_{in}	[mol/s]	inlet molar flow of acetone
F_{out}	[mol/s]	outlet molar flow of acetone
n	[–]	number of platelets
N	[–]	number of microchannels
[NL/h]		normal liters per hour
$S_{channel}$	[mm^2]	inner surface of each microchannel
S_{tot}	[mm^2]	total inner surface of the microchannels
S/V	[m^2/m^3]	surface/volume ratio of the microreactor
T_{50}	[°C]	temperature required to reach 50 % conversion
T_{95}	[°C]	temperature required to reach 95 % conversion
$V_{channel}$	[mm^3]	volume of each microchannel
V_{tot}	[mm^3]	total volume of the microchannels
$X_{/CO2}$	[–]	conversion of acetone calculated from carbon dioxide formation
$X_{/Acetone}$	[–]	conversion of acetone calculated from acetone disappearance

References

[1] S. V. Gokhale, R. K. Tayal, V. K. Jayaraman, B. D. Kulkarni, *Int. J. Chem. Reactor Eng.* **2005**, *3*, Review R2.
[2] V. Hessel, H. Löwe, *Chem. Eng. Technol.* **2003**, *26 (1)*, 13.
[3] V. Hessel, H. Löwe, *Chem. Eng. Technol.* **2003**, *26 (4)*, 391.
[4] L. Kiwi-Minsker, A. Renken, *Catal. Today* **2005**, *110*, 2.
[5] J. M. Commenge, L. Falk, J. P. Corriou, M. Matlosz, *Chem. Eng. Technol.* **2005**, *28 (4)*, 446.
[7] G. Kolb, V. Hessel, *Chem. Eng. J.* **2004**, *98*, 1.
[6] F. Sarrazin, L. Prat, N. Di Miceli, G. Cristobal, D. R. Link, D. A. Weitz, *Chem. Eng. Sci.* **2007**, *62*, 1042.
[8] A. O'Malley, B. K. Hodnett, *Catal. Today* **1999**, *54*, 31.
[9] D. Belpomme, P. Irigaray, L. Hardell, R. Clapp, L. Montagnier, S. Epstein, A. J. Sasco, *Environ. Res.* **2007**, *105 (3)*, 414.
[10] T. Schupp, H. M. Bolt, J. G. Hengstler, *Toxicology* **2005**, *206 (3)*, 461.
[11] V. S. Engleman, *Met. Finish.* **2000**, *98 (6)*, 433.
[12] F. I. Khan, A. K. Ghoshal, *J. Loss Prev. Process Ind.* **2000**, *13 (6)*, 527.
[13] J. J. Spivey, *Ind. Eng. Chem. Res.* **1987**, *26*, 2165.
[14] C. S. Henegan, G. J. Hutchings, S. H. Taylor, in *Catalysis*, (Eds: J. J. Spivey, G. W. Roberts), Vol. 17, The Royal Society of Chemistry, London **2004**.
[15] P. Papaefthimiou, T. Ioannides, X. E. Verykios, *Appl. Catal. B* **1997**, *13 (3/4)*, 175.
[16] J. Corella, J. M. Toledo, A. M Padilla, *Appl. Catal. B* **2000**, *27*, 243.

[17] A. Gil, M. A. Vicente, J.-F. Lambert, L. M. Gandia, *Catal. Today* **2001**, *68*, 41.
[18] S. Ordóñez, L. Bello, H. Sastre, R. Rosal, F. V. Diez, *Appl. Catal. B* **2002**, *38 (2)*, 139.
[19] J. J. Spivey, *Ind. Eng. Chem. Res.* **1987**, *26 (11)*, 2165.
[20] P. L. Mills, D. J. Quiram, J. F. Ryley, *Chem. Eng. Sci.* **2007**, *62 (24)*, 6992.
[21] F. Laermer, A. Schilp, *US Patent 5 501 893*, **1996**.
[22] N. Burgos, M. Paulis, M. M. Antxustegi, M. Montes, *Appl. Catal. B* **2002**, *38*, 251.
[23] R. K. Sharma, B. Zhou, S. Tong, K. T. Chuane, *Ind. Eng. Chem. Res.* **1995**, *34 (12)*, 4310.
[24] J. Tsou, P. Magnoux, M. Guisnet, J. J. M. Órfão, J. L. Figueiredo, *Appl. Catal. B* **2005**, *57 (2)*, 117.